Proceedings of the International Conference on Heat Exchanger Fouling and Cleaning - 2024 (Peer-reviewed)
April 21–26, 2024, Lisbon, Portugal; Editors: H.U. Zettler and E.M. Ishiyama

A MOVABLE HEATED FINGER DESIGN FOR THE MONITORING OF FOULING DURING POLYMER SYNTHESIS

***H. Huellemeier[1], W. Augustin[1] and S. Scholl[1]**
[1]Technische Universität Braunschweig, Institute for Chemical and Thermal Process Engineering,
Langer Kamp 7, 38106 Braunschweig, Germany (holly.huellemeier@tu-braunschweig.de)

ABSTRACT

The production of a latex dispersion by emulsion polymerization results in particle and reaction fouling of heat exchange surfaces. Fouling during emulsion polymerization deteriorates heat transfer efficiency, prevents continuous reactor configurations, and increases the frequency of cleaning operations. The investigation of fouling during emulsion polymerization is challenging due to the changes in the material properties of the bulk fluid during the course of the reaction.

This contribution presents the design of a reactor setup that employs an integrated movable heated finger for the study of fouling during emulsion polymerization. A heated finger with '*movable*' functionality has yet to be applied in previous fouling studies. This functionality has the potential to greatly reduce the experimental effort in the production of reaction fouling deposits for *ex-situ* analyses.

To identify key design parameters for a movable heated finger, preliminary design screening was first conducted with prototype heated fingers. The design screening emphasized considerations such as the type of heat supply (electric vs. fluidic) and the uniformity of the heat flow. Experiments involving the retraction of the prototype heated fingers from a polymer dispersion during fouling demonstrated the need to decouple the changes in the overall heat transfer coefficient due to fouling versus the changes due to retraction of the finger into air.

The preliminary design screening motivated a redesigned heated finger which was commissioned using various tests to characterize the heat flow in water and quantify the fouling of a preformed latex. The commissioning tests for the redesigned heated finger demonstrated the following: (1) a significant impact of the surface area of the finger in air on the heat required to maintain a constant surface temperature in liquid, (2) a higher fouling rate with a constant heat flux operation than a constant surface temperature operation, and (3) a dependence of the value of the convective heat transfer coefficient on the retraction height of the finger.

Discrepancies between the experimental and theoretical convective heat transfer coefficients emphasize the need to reevaluate the significance of axial heat flow in further development of the movable heated finger design. Ultimately, the successful implementation of a movable heated finger provides a method to create a time lapse of the fouling process along the length of the finger within a single experiment.

INTRODUCTION

Fouling during polymer synthesis

Many paints, coatings, and adhesives are produced through a process known as emulsion polymerization. In emulsion polymerization, monomers are polymerized in the form of an emulsion or a colloidal dispersion. [1] During the synthesis of these colloidal dispersions (also more commonly referred to as *latexes*), reacting and fully-reacted species come into contact with numerous processing surfaces (e.g., internal reactor walls, agitator surfaces, heat exchangers, pump internals, etc.). These surfaces may be heated or cooled depending on the progress of the reaction or the location within the processing line (i.e., pre- or post-processing). The temperature difference between these surfaces and the bulk fluid induces fouling which impairs heat transfer. [2,3] Consequently, fouling hinders the continuous dissipation of heat during an exothermic polymerization reaction. Heat dissipation is essential for process safety and product quality. To recover heat transfer efficiency after fouling has occurred, time-consuming cleaning processes are needed which result in a loss in productivity and large volumes of hazardous waste. [4]

It has been hypothesized that fouling during polymer synthesis can be classified as reaction and particle fouling. These classifications have motivated studies which differentiate *polymerization* fouling from a reacting solution (i.e., reaction fouling) and *polymer* fouling from a fully-reacted polymer dispersion (i.e., particle fouling). [2-6] Significant differences have been identified in the structure and topography of deposits from polymerization and polymer fouling. These differences warrant further investigation of the mechanisms of polymerization and polymer fouling. [3,6]

ISBN: 978-0-9984188-3-4; Published online www.heatexchanger-fouling.com

Furthermore, the progress of an emulsion polymerization reaction is hypothesized to significantly affect the rate of fouling. This effect may be impacted by the changes in the material properties of the bulk fluid along the course of a reaction, including increases in density, viscosity, and particle size with increasing conversion/solids content. [6] Additionally, some researchers have observed with a quartz crystal microbalance (QCM) that a thin, stable fouling layer, formed during the early stages of an emulsion polymerization reaction, may 'passivate' the surface against fouling occurring later during a reaction. [7] Furthermore, other researchers have suggested that most of the fouling occurs at the end of an emulsion polymerization reaction when the solids content is high; but these researchers also noted that there has been little focus on the conditioning of the surface during the early stages of a reaction. [2] Therefore, this study seeks to develop methods which can be used to understand how the formation of fouling layers or conditioning of the surface during the early stages of a reaction impact later fouling events.

Application of heated and cooled fingers

There are numerous methods for monitoring fouling *in-situ* and generating fouling deposits for *ex-situ* analyses. Among these methods is the use of heated or cooled fingers. The label 'heated' or 'cooled' simply depends on whether the surface temperature of the finger is higher or lower than the temperature of the bulk fluid. In most applications, the finger or probe is positioned within a continuously stirred vessel and the temperature of the bulk fluid is controlled by an external heating/cooling mantle. Fouling is induced at the surface of the finger due to the temperature difference between the bulk fluid and the surface of the finger. Fouling can be monitored and quantified through various metrics, including changes in the surface temperature or heat input. The changes in these fouling metrics are induced by an increase in the thermal resistance at the surface of the finger due to the growth of a fouling layer. The metric used to monitor fouling depends on the source of heat (e.g., fluid or electric) and the mode of operation (e.g., constant heat flux or constant surface temperature).

There are several applications of heated or cooled fingers in literature. A fluidic cooled finger has been applied for the study of crystallization fouling. [8,9] Similarly, fluidic cooled fingers have been applied for the study of wax deposition during petroleum processing. [10,11] Furthermore, an electric heated finger from the research group associated with the authors of this manuscript has been applied for the study of crystallization fouling from calcium sulfate, [12] fouling of polymer dispersions, [13] and generation of high-temperature dairy foulants for cleaning studies. [14,15] In particular, some researchers have been successful in applying theoretical heat and mass transfer models to accurately describe experimental fouling results for a cooled finger. [8,9] The aforementioned applications of heated or cooled fingers feature different design aspects and experimental setups which must be carefully selected based on the targeted system of study. To the authors' knowledge, there are no literature sources which apply a heated or cooled finger for the study of emulsion polymerization fouling.

Additionally, all fingers in the aforementioned studies remain stationary in the vessel containing the model fouling fluid. Conversely, the implementation of a finger which can be stepwise retracted from a vessel may be advantageous for some applications. Fouling layers on the portion of a finger which has been retracted from a bulk fluid could be considered 'frozen in time'. This characterization assumes the fouling progress is halted in the fouling layers which are no longer in contact with the bulk fouling fluid. This 'movable' functionality may be especially helpful for the study of reaction fouling where the nature of the deposit can change rapidly with the course of a reaction. Furthermore, with a movable heated finger, a single experiment can be used to collect deposits at multiple time points along the length of the probe rather than the use of separate experiments for each time point. This would greatly reduce experimental effort. Therefore, this study also focuses on the implementation of a *retractable or movable* finger to promote the time-series collection of fouling deposits along the length of the finger.

The objectives of this work include the identification of important design criteria for a heated finger through the testing of several prototype heated fingers (Part A. Prototype fingers), and the design and commissioning of a *movable* heated finger for the study of fouling during emulsion polymerization (Part B. Redesigned finger).

MATERIALS AND METHODS

A. Prototype fingers

A1. Design and testing parameters

Two prototype fingers were tested to define the design parameters for a finger which is suitable for the study of emulsion polymerization fouling (Figure 1). The primary motivation for the use of these prototype fingers was to identify the optimal source of heat: fluid or electric.

ISBN: 978-0-9984188-3-4; Published online www.heatexchanger-fouling.com

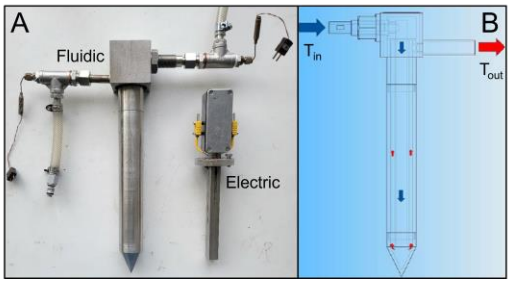

Figure 1. Prototype heated fingers: (A) Fluidic heated finger (left) and electric heated finger (right) side-by-side and (B) schematic of the internal flow pattern for the fluidic finger.

The fluidic finger (Figure 1A, left) is cylindrical (L = 300 mm and D_o = 40 mm) with a heat transfer area (A_s) of 0.021 m^2. The finger can be heated or cooled by fluid which enters and exits at the top of the finger. The inlet and outlet fluid temperatures are measured with T-type thermocouples (tolerance of ± 0.5 °C). The heating or cooling fluid enters the finger and travels down a pipe positioned at the center of the finger (D_i = 15.5 mm, Re_{in} ≈ 12,000). Upon reaching the bottom of the finger, the fluid path reverses direction and the return fluid is brought up along the outside of the center inlet pipe. This results in an annular flow pattern for the outlet (D_i = 20 mm, D_o = 34 mm, Re_{out} ≈ 3,500) (Figure 1B). The external surfaces are constructed of stainless steel. Heating water was supplied to the finger by a thermostat at a constant volumetric flow rate of 3.9 L/min. This finger was operated with a *constant inlet temperature* (T_{in} = 65–70 °C) which was controlled by an external thermostat. Changes in the heating fluid outlet temperature (T_{out}) were used to monitor fouling. The finger was positioned in a 7 L jacketed vessel which was continuously agitated by an overhead anchor-type stirrer. The bulk temperature of the fouling fluid was maintained at a constant value of 30 °C by an external thermostat. Retraction of this finger was tested with retraction steps of 35 mm every 30 min.

The electric heated finger (Figure 1A, right), which has been applied in several previous fouling studies, [12-15] is a rectangular prism (L = 175 mm, W = 20 mm, H = 15 mm). Heat is supplied by an electric heating rod (H10X100X350, Acim Jouanin, Evreux, FR) embedded in the center of the stainless steel housing. On two faces of the finger, K-type thermocouples (tolerance of ± 1.5 °C) are embedded within the surface of the stainless steel housing. Stainless steel sample plates (80 x 20 x 2 mm) were clamped onto these faces for easy extraction of the fouling layers. The total heat transfer area is assumed to be the surface area of the two sample plates (A_s = 0.0032 m^2). This finger was tested with two operation modes: (1) *constant surface temperature* (T_s = 70 °C), and (2) *constant heat flux* ($\dot{q}$ = 25 kW/m^2 or $\dot{Q}$ = 80 W).

For constant heat flux control of the electric prototype finger, the effective power is PID-controlled with LabView (2015, National Instruments, Austin, TX, USA) via a power meter (HM8115-2, Hameg Instruments, Mainhausen, DE). The input signal to the power meter is delivered by the transformation of a 0–10 VDC signal from an Agilent Multimeter (34970A, Keysight, Santa Rosa, CA, USA) to a 0–230 VAC signal through the use of a custom-built thyristor. Additionally, a custom-built temperature limiter is implemented between the communication of the thyristor and power-meter to read the internal temperature of the heating rod and shut down the heating rod in the case of overheating. For constant surface temperature control of the electric prototype finger, a temperature signal from the thermocouples embedded in the surface of the finger provides an input to the Agilent Multimeter. The power delivered to the heating rod is PID-controlled via LabView to adjust the surface temperature.

Tests with the electric prototype finger were conducted in a 2.5 L jacketed vessel which was continuously agitated by an overhead propellor-type stirrer. The bulk temperature of the fouling fluid was maintained at a constant value of 30 °C by an external thermostat. Retraction of this finger was tested with retraction steps of 10 mm every 30 min.

The model fouling fluid for the tests with both prototype fingers was performed with VINNAPAS LL6999 (Wacker Chemie AG, Munich, DE), a fully reacted, commercially-available vinyl acetate/ethylene copolymer dispersion. Both of the prototype fingers were operated in 'heated' mode for testing, meaning the surface temperature of the finger was greater than the bulk liquid temperature. An Agilent Multimeter (34970A, Keysight) was employed as the measuring scan device and LabView (2015, National Instruments) was employed for data acquisition.

A2. Data analysis

A.2.1 Fluidic finger: constant inlet temperature

The overall heat transfer coefficient (U, W/m^2·K) for the fluidic heated finger under steady state conditions can be described as,

$$U = \frac{\dot{V}\rho c_p}{A_s} \cdot \ln\left(\frac{T_i - T_b}{T_o - T_b}\right) \quad (1)$$

where $\dot{V}$ is the volumetric flow rate (m^3/s), ρ is the density (kg/m^3), c_p is the specific heat (J/kg·K), A_s is the heat transfer area (m^2), T_i and T_o are the inlet and outlet temperatures (°C) of water flowing through the finger, respectively, and T_b is the bulk temperature of the polymer dispersion in the vessel. Specifically, the outlet temperature is monitored as a function of time ($T_o(t)$) to describe the rate of fouling. The density (ρ) and specific heat (c_p) of water at 65 °C were assumed constant for the calculation as 980 kg/m^3 and 4190 J/kg·K, respectively. [16]

ISBN: 978-0-9984188-3-4; Published online www.heatexchanger-fouling.com

A.2.2 Electric finger: constant surface temperature and heat flux

The overall heat transfer coefficient for the electric heated finger under steady state conditions can be described as,

$$U = \frac{\dot{Q}}{A_s(T_s - T_b)} \quad (2)$$

Where $\dot{Q}$ is the heat supplied to the finger (W) and T_s is the surface temperature of the finger (°C). For the constant surface temperature operation, the change in power with time is used to monitor fouling ($\dot{Q}(t)$). While for the constant heat flux operation, the change in surface temperature with time is used to monitor fouling ($T_s(t)$).

For both prototype fingers, the integral thermal fouling resistance R_f (m²·K/W) can be calculated as the change in the overall heat transfer coefficient:

$$R_f(t) = \frac{1}{U_f(t)} - \frac{1}{U_0} \quad (3)$$

The initial heat transfer coefficient (U_0) was estimated as the y-intercept of a linear fit of $U_f(t)$. The start time of the fouling trial was identified based on the time of initial stabilization of the inlet temperature (T_{in}) for the fluidic finger and initial stabilization of the surface temperature (T_s) for the electric finger. Stabilization in temperature was identified as the initial minimum in the standard deviation of the temperature measurement which was calculated over a moving window. From the identified start time, the initial value of $R_f(t)$ was forced to 0 m²·K/W. All data was analyzed using MATLAB (R2022B, version 9.13.0.2049777, MathWorks, Natick, MA, USA).

B. Redesigned finger

B1. Design

Results from pretests with the prototype fingers (see *Results & Discussion*: *A. Prototype heated fingers*) motivated a redesigned heated finger (Figure 2).

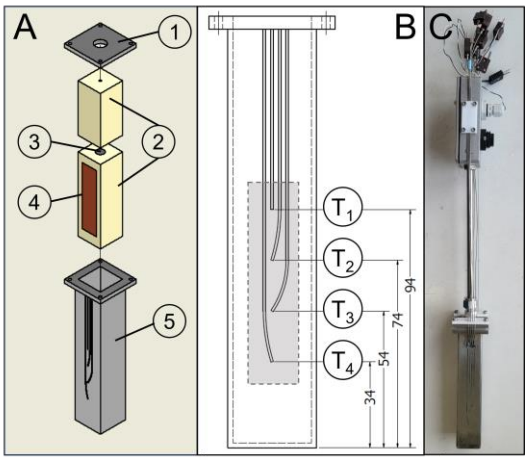

Figure 2. Redesigned heated finger. (A) Exploded view including (1) a stainless steel lid, (2) PEEK isolation blocks, (3) an electric heating rod, (4) a copper block, and (5) a stainless steel housing. (B) Side view of thermocouple placement. The shaded region describes the location of the sample plates. The dimensions are in mm. (C) Preliminary construction with the electrical connections and an extension rod for lowering the finger into the reaction vessel.

The redesigned finger is electrically heated and features several design modifications compared to the prototype electric heated finger (Figure 1A). The rationale for the selection of an electric heat source as opposed to a fluidic heat source is described in the section *Results and Discussion: B. Redesigned heated finger*. The redesigned finger has PEEK isolation around the heat transfer surfaces to precisely define the heat transfer area as the area of the sample plates and provide insulation. The heating rod (maximum power of 350 W, HJ10X100X350W, Acim Jouanin) is embedded in a copper block which ensures an even heat distribution. The components of the finger are fixed inside a stainless steel housing by a thermal grease which has a melting temperature of 250 °C (Figure 2A). The finger features two faces where sample plates (80 x 20 x 2 mm) can be clamped. Behind each sample plate, there are four T-type thermocouples (tolerance of ± 0.5 °C, 1TV10SMPM500, TMH, Maintal, DE). The thermocouples are positioned at different, equally spaced heights. This results in a total of eight thermocouples for surface temperature measurements (Figure 2B). To eliminate uncertainty in the temperature measurements, all thermocouples were calibrated before experimentation.

The control principle for the different operation modes (constant heat flux and constant surface temperature) is the same as the prototype electric finger (see section *A1. Prototype fingers*). An Agilent Multimeter (34970A, Keysight) was employed as the measuring scan device and LabView (2015, National Instruments) was employed for data acquisition. Additionally, the finger has an extension arm connected to a manual linear axis (SHT-12 DS 10x3, drylin®, igus GmbH, Cologne, DE) which allows it to be lowered into the reaction vessel. The extension arm also allows the electrical connections to be isolated outside the lid of the reaction vessel (Figure 2C).

B2. Commissioning tests

The redesigned heated finger was commissioned using various tests which evaluated the performance of the redesigned finger with different bulk fluids (water vs. preformed latex) and different functionalities (no retraction vs. retraction, constant heat flux vs. constant surface temperature). These tests provide the foundation for the future use of the redesigned heated finger to study fouling during an emulsion polymerization reaction with retraction. Data for the commissioning tests were

ISBN: 978-0-9984188-3-4; Published online www.heatexchanger-fouling.com

analyzed using MATLAB (R2022B, version 9.13.0.2049777).

B2.1 Commissioning Test #1: water without and with retraction

For *Commissioning Test #1*, the finger was positioned in a jacketed 5 L glass reaction vessel with an inner diameter of 180 mm. The fouling fluid was continuously agitated by an anchor stirrer at 200 RPM. Additional details regarding the experimental setup are described in Figure 3.

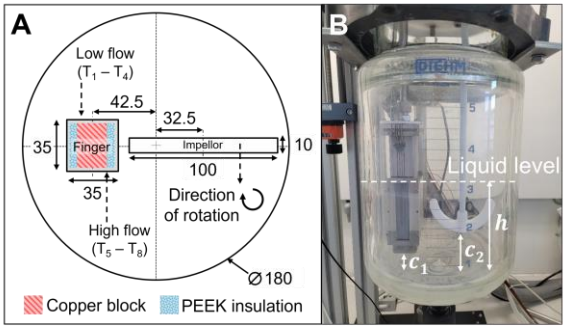

Figure 3. Experimental setup for the commissioning tests: (A) Top view of reactor. Sketch is to scale with all dimensions in mm. Embedded in the low flow face (in the wake of agitator motion) are thermocouples $T_1 - T_4$, while embedded in the high flow face are thermocouples $T_5 - T_8$. (B) Front view of reactor with $c_1 = 9$ mm, $c_2 = 36$ mm, and $h = 124$ mm.

Commissioning Test #1 was conducted at a constant bulk temperature (T_b) of 55 °C resulting in a Reynolds number of ~39,000 assuming a density (ρ) and dynamic viscosity (μ) for water of 985.7 kg/m^3 and 0.5 mPa·s, respectively [16] (note: the Reynolds number for a stirred vessel was calculated as $Re = nd^2\rho/\mu$ where n is the RPM of the agitator, d is the diameter of the agitator, ρ is the density of the bulk fluid, and μ is the dynamic viscosity of the bulk fluid). The bulk temperature was controlled by an external thermostat connected to the jacket of the reactor with feedback control from a Pt100 RTD sensor in the reactor. Stainless steel (1.4301) sample plates were positioned on the finger as described by the shaded region in Figure 2B. The sample plates were clamped to the surface of the finger with a stainless steel clamp. The finger was tested with a constant surface temperature (T_s) of 70 °C. Upon full submersion of the sample plates in water, the thermocouple selected for temperature control was T_1 (Figure 2B), which is on the 'low flow face' (Figure 3A). Additionally, the temperature and power profiles were collected with retraction steps of 20 mm every 30 mins. During retraction, the temperature control point was switched to the thermocouple that was closest, yet still below, the surface of the liquid (i.e., 0 mm retraction = T_1, 20 mm retraction = T_2, etc.)

B2.2 Commissioning Test #2: preformed latex without retraction

Commissioning Test #2 was conducted to evaluate the ability of the redesigned heated finger to detect fouling of an emulsion polymer. For this test, a vinyl acetate/vinyl ester copolymer was selected as the model fouling system. The model system is a co-polymer dispersion with vinyl acetate (VAc) and vinyl neodecanoate (VeoVa10) as the monomers in a weight ratio of VAc:VeoVa10 of 80:20. The dispersion was produced in a pilot plant facility by Wacker Chemie AG with a final solids content of 54.5%. Polymerization was initiated by a reducing agent, Brüggolit, and an oxidizing agent, tert-butyl hydroperoxide (TBHP), with polyvinyl alcohol (PVA) as an emulsifier at a concentration of 8 % wt. PVA/wt. monomer. The dispersion was diluted with distilled water to a solids content of 30 % for fouling tests.

Fouling tests with the redesigned finger were conducted at a constant bulk temperature (T_b) of 24 °C using an external thermostat. The reactor was configured like the setup depicted in Figure 3, except for modification of the positions described in Figure 3B to increase flow below the finger ($c_1 = 33$ mm, $c_2 = 33$ mm, $h = 140$ mm). The Reynolds number was calculated as ~200 with an estimated viscosity and density of 1030 kg/m^3 and 0.1 Pa·s, respectively, based on the work of [3] for a similar VAc-based latex at a 30% solids content. Furthermore, compared to the commissioning tests described in section B2.1, the sample plate clamp material was switched from stainless steel to PEEK to reduce heat losses on the surfaces of the finger which surround the sample plates.

Similar to the electric prototype finger, two operation modes were evaluated for the redesigned finger: (1) constant surface temperature (T_s = 74 °C) and (2) constant heat flux ($\dot{q}$ = 38.1 kW/m^2 or $\dot{Q}$ = 122 W). The constant heat flux condition was selected to produce an initial surface temperature (~73 °C) which was close to the constant surface temperature condition (74 °C). Three experiments were performed for each operating condition ($n = 3$) and fouling runs were conducted for at least 60 mins. Stainless steel sample plates (1.4301) were clamped to the surface. For the calculation of the fouling resistance (R_f), Eqs. (2) and (3) were applied with an assumed heat transfer surface area equal to the combined surface area of the two sample plates (A_s = 0.0032 m^2). Additionally, it was assumed that all of the supplied heat ($\dot{Q}$) was transferred through the surface area of the plate (i.e., no heat losses) and the heat was evenly distributed across the heat transfer surface area. The overall heat transfer coefficient (U) and thus the fouling resistance (R_f) were evaluated separately for the low and high flow faces, where T_s was calculated as the average of the four surface embedded thermocouples on the respective face.

ISBN: 978-0-9984188-3-4; Published online www.heatexchanger-fouling.com

The initial heat transfer coefficient (U_0) was estimated as the y-intercept of a linear fit of $U_f(t)$. The time for the start of the calculation of R_f was selected based on the initial stabilization of T_1 after switching on the heat supply. The stabilization of T_1 was identified as the initial minimum in the standard deviation of the temperature measurement calculated over a moving window. From the identified start time, the value of R_f was forced to 0 m^2·K/W .

B2.3 Commissioning Test #3: water and artificial fouling layers without and with retraction

Commissioning Test #3 was designed to better understand the heat transfer situation associated with the redesigned heated finger. During a polymerization reaction, the redesigned heated finger will be moved out of the reacting solution in discrete steps. This procedure is expected to produce a fouling resistance versus time curve similar to the sketch described in Figure 4A. In this sketch, it is notable that the fouling resistance (R_f) increases with the addition of subsequent fouling layers onto the surface area submerged under the liquid level during a finite time (i.e., t_0 to t_1, t_1 to t_2, etc.). But R_f remains unchanged during the retraction steps which occur over a small time interval (i.e., $dT \approx 0$). Additionally, a linear change in R_f with time (i.e., a constant fouling rate) is depicted for simplicity, but other time-dependent behaviors in the change in R_f are possible (i.e., asymptotic).

Yet to achieve the goal described in Figure 4A, additional information, including the heat losses and the convective heat transfer coefficient in liquid, must be quantified. Therefore, a calibration procedure with artificial fouling layers is proposed in *Commissioning Test #3*. In summary, the calibration procedure transforms the sketch described in Figure 4A to the sketch in Figure 4B, such that the temperature change associated with the steady state heat transfer at different retraction heights (h) is used to evaluate the relevant heat transfer parameters. Similar to Figure 4A, a change in R_f in Figure 4B is associated with the addition of subsequent fouling layers, but R_f remains unchanged during the retraction steps.

To explain the calibration procedure, the situation at h_0 in Figure 4B is detailed in Figure 5. The change in the surface temperature associated with the addition of R_{f1} (Figure 4B) can be evaluated by comparing the difference in the surface temperature between a clean state (Figure 5A) and an artificially fouled state (Figure 5B). For the artificial fouling layer, a 0.5 mm thick PTFE film is applied to the surface of the stainless steel sample plate.

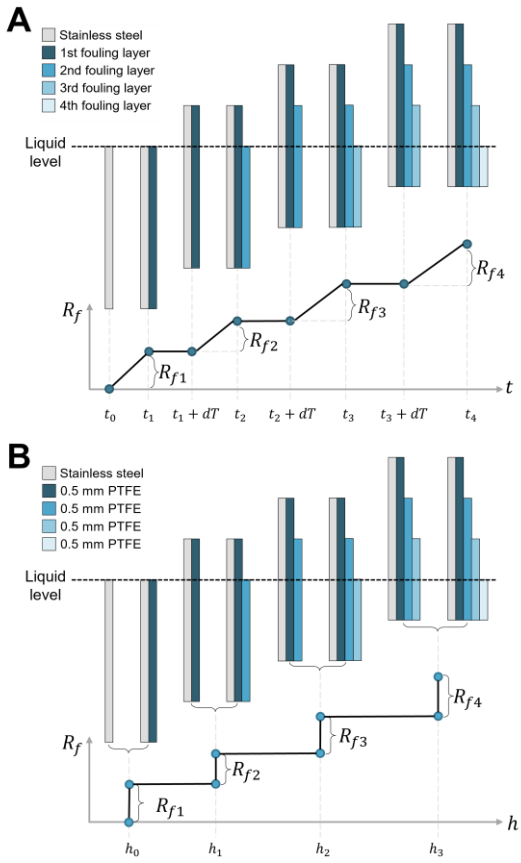

Figure 4. Overview of the stepwise thermal resistance curve for a stainless steel sample plate on one side of the movable heated finger: (A) Expected fouling resistance (R_f) versus reaction time (t) behavior assuming a constant fouling rate and (B) the evaluation of the steady state change in fouling resistance with the addition of artificial fouling layers (0.5 mm thick PTFE layers) at different retraction heights (h) for the calibration procedure.

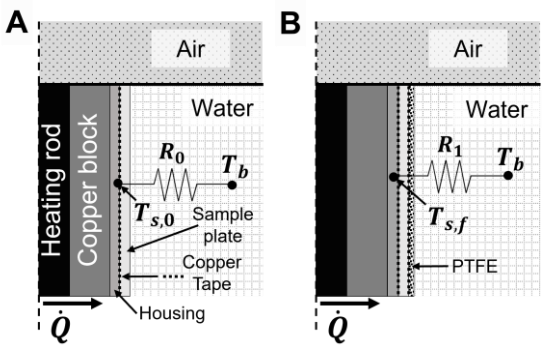

Figure 5. Comparison of the thermal resistance networks for the clean and fouled states: (A) Clean state with the surface and bulk temperatures of $T_{s,0}$ and T_b, respectively. The dotted line represents the copper tape between the sample plate and the stainless steel housing. The total resistance between $T_{s,0}$ and T_b, is R_0. (B) An artificially fouled state with a fouled surface temperature of $T_{s,f}$ and the addition of 0,5 mm of PTFE. Note the addition of a layer of copper tape between the PTFE and the sample plate. In both (A) and (B), $\dot{Q}$ is the heat flow through surface area of the sample plate submerged in water.

ISBN: 978-0-9984188-3-4; Published online www.heatexchanger-fouling.com

The thermal contact resistance between the stainless steel sample plate and the surface of the finger is reduced by the use of a double sided copper tape. The tape consists of a copper foil with a thin layer of acrylic adhesive on each side (Copper Foil EMI Shielding Tape #1182, 3M, St. Paul, MN, USA). Additionally, this copper tape is used to adhere the artificial PTFE fouling layer to the surface of the sample plate. The thermal resistance network associated with the conductive heat transport at the surface of the finger can be evaluated by using the material properties described in Table 1.

Table 1. Material properties for the thermal resistance calculations

Material		Thickness (mm)	Thermal conductivity (W/m·K) [17]	Thermal resistance (× 10^{-3} m²·K/W)
Copper Tape	Copper Foil	0.035	401	0.27
	Acrylic adhesive	0.054*	0.2	
Stainless steel		2	15	0.13
PTFE		0.5	0.25	2.0

*Combined thickness for doubled-sided tape

The calibration protocol assumes that the heat flow through the sample plate ($\dot{Q}$, Figure 5) and surface area of heat transfer is the same for both states (clean and artificially fouled) at any given retraction step. With these assumptions, the convective heat transfer coefficient (h_{conv}) can be evaluated by the dimensionless temperature ratio (θ_T) (Eq. 4):

$$\theta_T = \frac{U_0}{U_f} = \frac{(T_{s,f} - T_b)}{(T_{s,0} - T_b)} = \frac{\frac{1}{h_{conv}} + R_1}{\frac{1}{h_{conv}} + R_0} \qquad (4)$$

Where U_0 and U_f are the overall heat transfer coefficients of the clean and fouled states, respectively; $T_{s,f}$ and $T_{s,0}$ are the average surface temperatures of the clean and fouled states in liquid, respectively; T_b is the bulk fluid temperature; and R_0 and R_1 are the conductive thermal resistances associated with the clean and fouled states, respectively. The latter conductive thermal resistances of the clean (R_0) and fouled (R_1) states were estimated as 0.40×10^{-3} and 2.67×10^{-3} m²K/W, respectively, based on the values described in Table 1. The same reactor configuration associated with *Commissioning Test #2* was applied for the calibration. The effects of the power level (26.8, 35.7, 44.6, and 53.7 W) and the retraction height (0, 20, 40 mm) on the value of h_{conv} were evaluated during the calibration procedure. Water was selected as the bulk fluid and the bulk temperature was held constant (T_b = 64 °C) by controlling the temperature of the mantle of the vessel with an external thermostat. This bulk temperature was selected because it is the bulk temperature of the emulsion polymerization reaction that is planned for future studies. With the agitator setup described in *Commissioning Test #2*, the Reynolds number was estimated as ~45,000.

RESULTS AND DISCUSSION

A. Prototype fingers

Fouling without retraction

Figure 6 describes the change in the integral fouling resistance with time for both prototype fingers under different operating conditions without retraction.

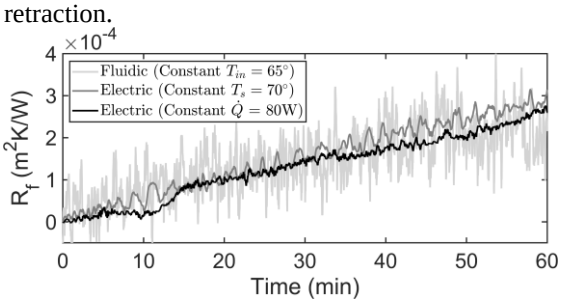

Figure 6. Fouling resistance as a function of time for the fluidic and electric prototype heated fingers without movement and with VINNAPAS LL 6999 as the model fouling fluid at a bulk temperature of 30 °C. All data has been filtered with a Savitzky–Golay filter of 3rd order and window length ≈ 22 s.

During the 60 min fouling period described in Figure 6, both prototype fingers at all operating conditions demonstrate a constant fouling rate as described by the linear rise in $R_f(t)$. Furthermore, the results show similar magnitudes in $R_f(t)$. For the electric finger, it is unexpected that both operating conditions would show similar fouling behaviors. The expected difference in behavior can be explained by considering steady state heat transfer theory with a constant external resistance to heat transfer. During constant heat flux operation, the temperature of the surface of the fouling deposit, exposed to bulk fluid flow, is expected to remain constant as the temperature behind the sample plate increases. [18] This results in a constant temperature gradient between the bulk fluid and the surface of the deposit. The temperature gradient between a heated surface and the bulk fluid, has been cited as one of the driving forces for polymer fouling. [3,6] Therefore, in Figure 6, the fact that constant heat flux operation imposes a constant temperature gradient and thus, results in a linear increase of R_f with time follows expectations.

In contrast, during constant surface temperature operation for the electric finger, the surface temperature of the fouling deposit, exposed to bulk fluid flow, is expected to decrease with increasing deposit layer thickness as the temperature behind the

ISBN: 978-0-9984188-3-4; Published online www.heatexchanger-fouling.com

sample plate remains constant. Assuming the temperature gradient between the deposit surface and the bulk fluid is a significant driving force for polymer fouling, it would be expected that the fouling rate would decrease with time. Therefore, the $R_f(t)$ curve depicted in Figure 6 might be expected to show an asymptotic behavior, rather than a linear behavior for the constant surface temperature operation. Yet, this behavior is not observed in these data. Such behavior may be initiated at longer run times and thus greater fouling layer thicknesses.

The prototype fluidic finger demonstrates a similar magnitude in the change in R_f with time when compared to the electric prototype finger. But a quantitative comparison between the electric and fluidic fingers is difficult due to the differences in the geometries and experimental setups (e.g., vessel volume and agitator type). Despite this challenge, the uniformity of the fouling deposits and the data quality of the fluidic finger can still be evaluated in comparison to the electric finger. The fluidic finger showed greater nonuniformity in the pattern of the fouling deposits on the surface of the finger when compared to the deposits on the electric finger (pictures of the fouling deposits are not shown). This may be due to the large size of the fluidic finger compared to the size of the vessel. The ratio of the volume of vessel to volume of the fluidic finger is 27.1, whereas for other fluidic finger applications the ratio is almost double (55.2, [8,9]). The large size of the prototype fluidic finger compared to the size of the vessel may greatly disrupt flow patterns in the vessel resulting in a non-uniform fouling behavior at the surface.

Furthermore, the data associated with the fluidic finger demonstrates high levels of noise when compared with the noise of the data of the electric finger (with the same level of data filtering). This suggests the need to limit noise in the temperature signal and ensure that there is adequate sensitivity for the thermocouples at the inlet and outlet of a fluidic finger such that small changes in the temperatures can be detected for correspondingly small changes in the thermal resistance of the fouling layer.

A holistic evaluation of the source of heat supply (electric vs. fluid) for the finger is limited by the differences in the prototype fingers compared in this study, including their differences in size and geometry. Additionally, a lack of sensors enabling control of the heat flux or surface temperature of the fluidic finger further limits comparison between the finger types. The latter limitation could be overcome by embedding a thermocouple or heat flux sensor in surface of the fluidic finger for feedback control to the heating water. Despite these limitations, the results from the prototype fingers without retraction demonstrated quantifiable fouling resistance for both prototype fingers under all operating conditions.

Fouling with retraction

During retraction, the prototype fingers demonstrate different behaviors in their characteristic fouling metrics (i.e., temperature or power) depending on the mode of operation and the source of heat (Figure 7). Data from both fingers show patterns associated with fouling when the finger is stationary (i.e., 0–30 min, 30–60 min, and 60–90 min) and exhibit a ‘stair-step’ pattern with each retraction step (i.e., at 30 and at 60 min).

For the electric finger at a constant surface temperature, the power level decreases with fouling during each stationary period (Figure 7A). This is due to the effective increase in ‘insulation’ at the surface of the finger (i.e., increasing thermal resistance) during fouling. This insulation results in a decrease in the heat demand required to maintain a constant surface temperature behind the sample plate. With each retraction step, the power required to keep the surface temperature at 70 °C exhibits a ‘step-down’ (Figure 7A). It is expected that when the finger is retracted, heat flow will be concentrated to the liquid phase (polymer solution) rather than to the gas phase (air). This expectation is supported by the fact that the gas phase has a much lower convective heat transfer coefficient (i.e., high external resistance to heat transfer) than the convective heat transfer coefficient of the agitated liquid polymer solution (i.e., low external resistance to heat transfer). As a result, it is expected that heat will follow the path of least resistance and continue to travel into the liquid phase despite retraction into air. Additionally, retraction results in an effective reduction in the heat transfer surface area because the surface area retracted into air effectively becomes an insulator and there is a new, smaller heat transfer area in liquid. Assuming steady state heat transfer with no change in the overall heat transfer coefficient, a reduction in surface area will decrease the heat required to maintain a constant surface temperature.

Conversely, during constant heat flux operation the temperature of the thermocouple which is embedded in the surface of the finger behind the center of the sample plate, increases during each stationary period due to fouling (Figure 7B). This can also be explained by the effective ‘insulation’ (i.e., increasing thermal resistance) provided by the fouling layer as it grows in thickness. Additionally, at each retraction step, the surface temperature exhibits a ‘step-up’ (Figure 7B). This is due to the reduction in the effective heat transfer area in liquid with retraction which results in an increase in the heat flux in the liquid phase. Correspondingly, the increase in heat flux results in an increase in the surface temperature in the liquid phase. This behavior in the temperature curve supports the

ISBN: 978-0-9984188-3-4; Published online www.heatexchanger-fouling.com

previously discussed expectation that most of the heat is flowing into the liquid phase, rather than the gas phase. Furthermore, it is also notable that the rate of increase of the temperature curve within each stationary phase due to fouling increases with additional retraction steps. This suggests that the rate of fouling is proportional to the heat flux in the liquid phase.

Finally, for the fluidic finger (Figure 7C), trends in the temperature curves due to fouling during each stationary phase are less apparent than the fouling metrics for the electric finger (Figure 7A–B). With a constant inlet temperature for the fluidic finger, it would be expected that the outlet temperature would increase due to fouling. This behavior is hard to detect in Figure 7C, but this may be due to the high levels of noise in the temperature signal. Conversely, the behavior of the outlet temperature at each retraction step follows expectation by demonstrating a 'step-up'. With retraction, the reduction in the effective heat transfer area in liquid results in a decrease in the amount of heat lost from the heating water to the liquid polymer solution. Therefore, the outlet temperature of the heating water should increase at each retraction step.

These results can be used to calculate the change in the overall heat transfer coefficient with time for both fingers and at all operating conditions (Figure 8). As expected, the stair-step pattern of the fouling metrics is reflected in the overall heat transfer coefficient. This information cannot be directly used to calculate the fouling resistance as in Figure 6 because the change in heat flow to the liquid phase with retraction must be calculated. Additional information about the heat transfer situation (e.g., convective heat transfer coefficient and heat losses) is needed for this analysis.

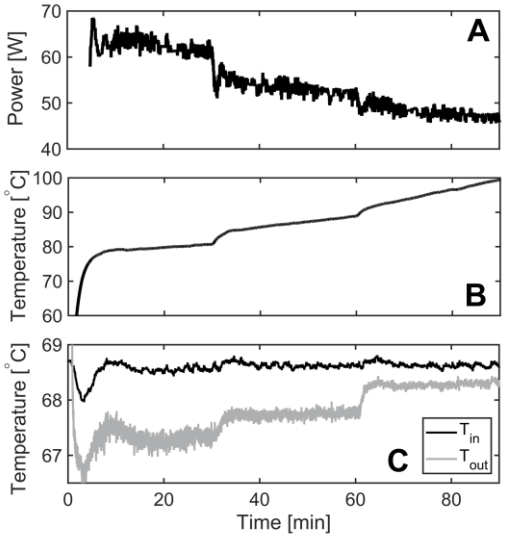

Figure 7. Change in the fouling metrics for the prototype fingers with retraction: (A) the electric finger with constant surface temperature of T_s = 70 °C and retraction steps of 10 mm every 30 min (note: initial data points have been excluded due to control fluctuations), (B) the electric finger with a constant heat flow of $\dot{Q} = 80$ W and retraction steps of 10 mm every 30 min, and (C) the fluidic finger with a constant inlet temperature of T_{in} = 70 °C with retraction steps of 35 mm every 30 min.

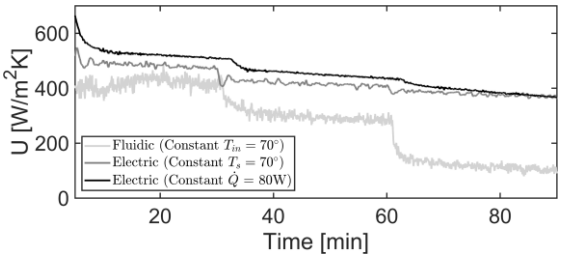

Figure 8. Change in the overall heat transfer coefficient with the retraction of the prototype heated fingers. All data has been filtered with a Savitzky–Golay filter of 3rd order and window length ≈ 13 s.

B. Redesigned finger

A new heated finger design was developed based on the results from the preliminary design screening of the prototype fingers. The electric prototype finger was selected as a model for the redesigned finger as opposed to the fluidic finger due to its versatility and ease-of-use with two modes of operation (constant surface temperature and constant heat flux), high data quality with minimal noise, rapid control response in the power level needed to maintain a constant surface temperature with retraction steps, and potential for supporting high sensitivity in the control of power in response to thin fouling layers. Finally, the geometry of the electric prototype finger enables the use of sample plates for easy fouling deposit extraction. The selection of an electric heated finger is oneed to heated applications *only*, rather than cooled *and* heated applications which are possible with a fluidic finger. But fouling rates on cooled surfaces ($T_s < T_b$) have been found to be very low compared to heated surfaces ($T_s > T_b$). [2,3,6] Therefore, the redesigned finger will focus on the most problematic fouling situation for emulsion polymerization applications which is fouling on heated surfaces.

Commissioning Test #1: water without and with retraction

The temperature (for the low-flow face) and power profiles for the redesigned finger with retraction from water into air are presented in Figure 9.

ISBN: 978-0-9984188-3-4; Published online www.heatexchanger-fouling.com

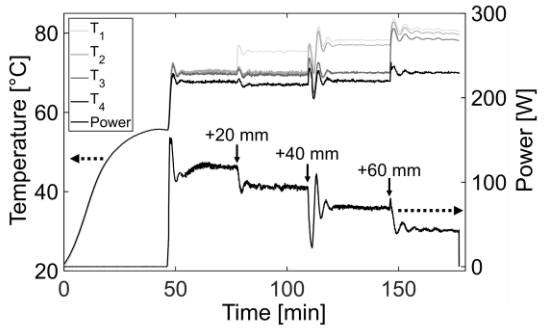

Figure 9. Power and temperature curves for the redesigned heated finger with retraction from water at T_b = 55 °C and T_s = 70 °C. The heated finger was retracted with steps of 20 mm every 30 min. The locations of $T_1 - T_4$ are identified on Figure 2 and located on the low flow face (Figure 3B). The power is distributed on both sides of the finger. The curves for $T_5 - T_8$ on the high flow face of the finger (Figure 3B) are not shown.

With the complete submersion of the finger in water and the start of the power supply ($t \approx 50$ min, Figure 9), the finger shows uniformity in its surface temperatures with an average temperature ± the absolute deviation for $T_1 - T_4$ equal to 70 ± 2 °C. This suggests a uniform distribution of heat along the full height (80 mm) of the sample plate (Figure 2). This is a significant improvement compared to the prototype electric finger where the temperature difference between a thermocouple positioned behind the center of the sample plate to a thermocouple positioned behind the top of the sample plate was measured to be 10–15 K (results not shown).

With the first retraction step (Δh = 20 mm, $t \approx 80$ min, Figure 9), the point of temperature control is switched from thermocouple T_1 to T_2 as the thermocouple associated with T_1 is exposed to the gas phase. The thermocouples below the surface of the liquid maintain uniformity near 70 °C. This trend continues until only T_4 remains under the surface of the liquid ($t \approx 150$ min, Figure 9). The temperatures of the thermocouples above the liquid surface do not rise dramatically which is important for limiting possible ageing and chemical changes in the fouling layers in the gas phase.

To understand how the power changes with the retraction of the finger, the average power level for each retraction step was determined from the data in Figure 9 and plotted against the heat transferring surface area (from both sides of the finger) exposed to air (Figure 10A). The results show a linear decrease in the power with an increasing surface area exposed to air. These results may suggest a negligible heat transfer to the gas phase with increasing retraction. This can be explained due to the main heat transfer mechanism in air being natural convection (low convective heat transfer coefficient) as opposed to the mechanism of forced convection in the stirred water (high convective heat transfer coefficient). Therefore, there is a lower resistance to heat transfer in water compared to air.

Additionally, given the temperature measurements at different heights along the length of the finger, the conductive axial heat flow ($\dot{Q}_{ij}$) can be estimated by Eq. 5 (Figure 10B):

$$\dot{Q}_{ij} = \frac{kA_c(T_i - T_j)}{z} \quad (5)$$

Where k is the thermal conductivity of the stainless steel housing (15 W/m·K, Table 1), A_c is the cross sectional area of the housing perpendicular to heat flow (4×10^{-5} m^2), $(T_i - T_j)$ is the temperature difference between thermocouples i and j (K), and z is the distance between points i and j (2×10^{-2} m). The axial heat flow upon full submersion of the finger in liquid is low (surface area in air of 0 cm^2, Figure 10B) as supported by the temperature uniformity prior to retraction (Figure 9). It is evident that the axial heat flow is maximized between the measurement points just above and below the surface during each phase of the retraction. Furthermore, the cumulative axial heat flow shows a continual increase, albeit with a decreasing rate.

The estimate of the axial heat flow described in Figure 10B is limited to one dimension of the stainless steel housing. Therefore, it may underestimate the actual magnitude of axial heat flow for the entire heated finger body. For an accurate estimation of the total axial heat flow across the full two-dimensional cross section of the body of the finger, the composite thermal conductivity of the layered construction of materials (i.e., copper, PEEK, thermal grease, stainless steel) and temperature distribution within the finger must be known. Therefore, it should be noted that Figure 10B represents the *trend* in axial heat flow with retraction, rather than the actual magnitude.

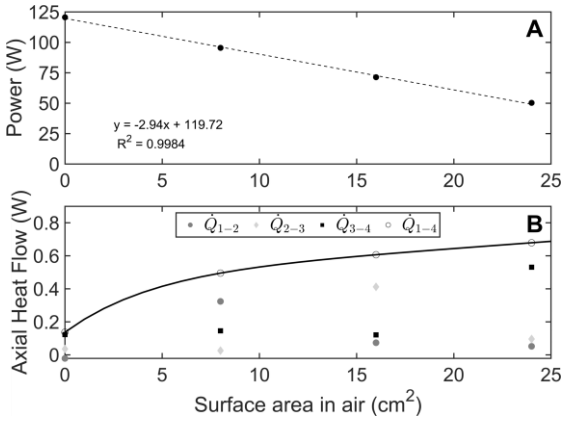

Figure 10. Change in power and axial heat flow as a function of surface area in air from both sides of finger with retraction of the redesigned heated finger. (A) The change in the average power for retraction steps of 2 cm every 30 min for both sides of finger from data in Figure 9 and (B) the axial heat flow for both sides of finger based on the temperature differences associated with thermocouple locations $T_1 - T_4$ (see Figure 2B) during the

ISBN: 978-0-9984188-3-4; Published online www.heatexchanger-fouling.com

finger retraction. The cumulative heat flow is plotted as a solid line.

Commissioning Test #2: preformed latex without retraction

The average change in R_f with time (n = 3) for the two operating conditions, constant surface temperature and constant heat flux, with the redesigned heated finger is described in Figure 11.

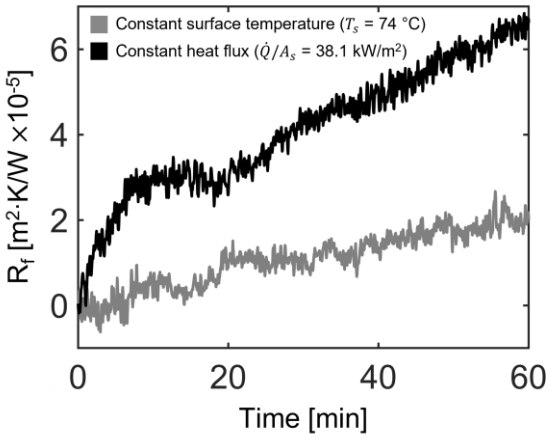

Figure 11. Change in fouling resistance (R_f) with time for two operating conditions with the redesigned finger. The data was evaluated using the surface temperature and thus overall heat transfer coefficient associated with the low flow face (n = 3). All data has been filtered with a Savitzky–Golay filter of 3rd order and window length ≈ 13 s. The start of the calculation of R_f is associated with the stabilization of the T_s after turning on the power supply (t_{start} ≈ 20 and 12 min for constant T_s and $\dot{Q}$, respectively).

The results show a higher fouling rate for the constant heat flux condition (average ± standard deviation = $8.56 \times 10^{-7} \pm 4.29 \times 10^{-7}$ m²·K/W·min) compared to the constant surface temperature condition (average ± standard deviation = $3.10 \times 10^{-7} \pm 6.70 \times 10^{-8}$ m²·K/W·min). The previous discussion of the expected differences in fouling behavior between constant heat flux and constant surface temperature modes of operation for the prototype electric finger (Figure 6) may help explain the difference in the rates of fouling described in Figure 11. The fouling rate for the constant surface temperature operation might be expected to be lower than the fouling rate for constant heat flux operation due to the decrease in the temperature gradient between the deposit surface and the bulk fluid with an increase in fouling layer thickness for the constant surface temperature operation.

In terms of operation with retraction, constant surface temperature operation is expected to be easier to control compared to constant heat flux operation. During constant surface temperature operation, only the point of temperature control must be switched with each retraction step as demonstrated in *Commissioning Test #1* (e.g., as T_1 is retracted into air with a 20 mm step, T_2 becomes the new point of temperature control of T_s in liquid). In comparison, constant heat flux control requires an evaluation of any changes in the internal conductive and external convective thermal resistances with retraction. This evaluation is needed to determine the new power level needed maintain a constant heat flux after a retraction step. But despite this challenge in control, the constant heat flux operation results in a higher fouling rate (i.e., 'worst case' fouling situation) than the constant surface temperature operation. If the 'worst case' fouling situation is to be evaluated, a better understanding of the heat transfer situation is needed. Addressing this need provides the motivation for *Commissioning Test #3*.

Commissioning Test #3: water and artificial fouling layers without and with retraction

During the calibration protocol associated with *Commissioning Test #3*, the difference in the surface temperature in liquid between clean and artificially fouled states was compared to determine the estimated heat flow through the sample plate and the convective heat transfer coefficient. The difference in the surface temperatures between the two calibration states is compared in Figure 12.

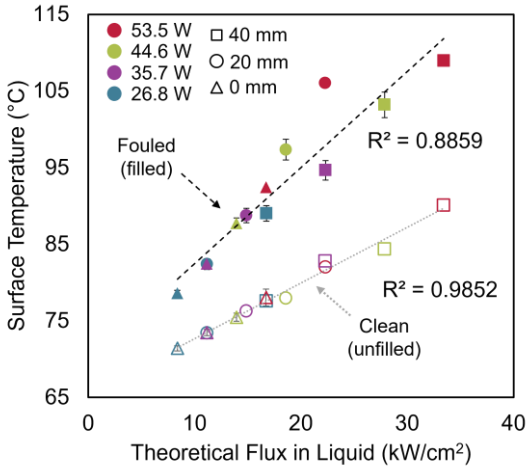

Figure 12. Surface temperature in liquid for clean (unfilled markers) and artificially fouled (filled markers) states as a function of the theoretical flux in liquid at different power levels (identified by marker color) and retraction heights (identified by marker shape). The theoretical flux in liquid is equal to supplied heat divided by the surface area of the sample plate submerged in water. For 26.8–44.6 W, the replication for fouled state is n = 3 at all retraction heights and the replication for the clean samples at 0 mm is n = 2. All other conditions and data associated with 53.5 W have n = 1.

The data in Figure 12 describe a direct relationship between the surface temperature in liquid and the theoretical heat flux in liquid. Furthermore, the data points overlap at different combinations of the experimental variables (power and retraction height) when the theoretical flux is

ISBN: 978-0-9984188-3-4; Published online www.heatexchanger-fouling.com

constant. The results in Figure 12 were used to calculate the dimensionless temperature difference described in Eq. 4 and thus, estimate the convective heat transfer coefficient (h_{conv}). The results are plotted in Figure 13A. Additionally, the heat losses are derived (Figure 13B).

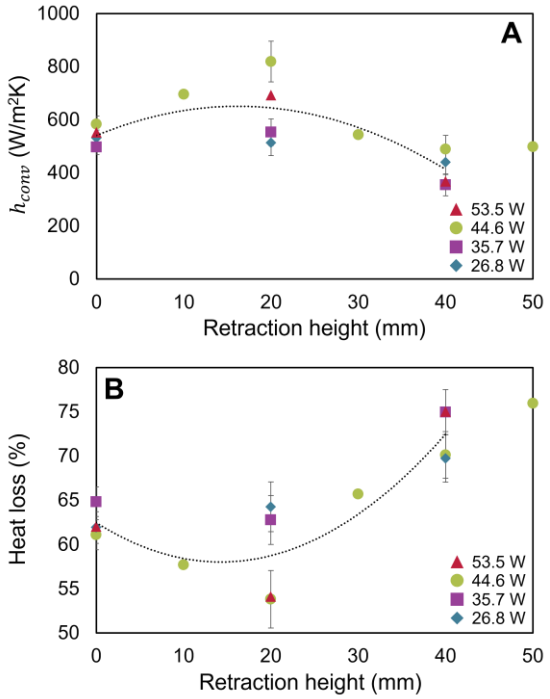

Figure 13. (A) Estimated convective heat transfer coefficient and (B) heat losses calculated from the calibration protocol at different power levels and retraction heights. A polynomial fit is applied to the data associated with retraction heights of 0, 20, and 40 mm to illustrate trends.

The results in Figure 13 illustrate that the estimated h_{conv} and the heat losses depend on the retraction height with a maximum and minimum in h_{conv} and the heat losses, respectively between a retraction level of 10 and 20 mm. This is may be due to a change in the fluid dynamics in the vessel with retraction of the finger. Upon full submersion, the finger displaces liquid and results in an obstruction to flow. Upon retraction, the liquid displacement and flow obstruction is reduced which may impact h_{conv}. Data points at intermediate retraction heights (10, 30, and 50 mm) at one power level (44.6 W) were collected to confirm this trend. Additionally, the results estimate significant heat losses (> 60%) (Figure 13B). An accurate estimation of the heat losses is needed to calculate the actual fouling resistance.

The theoretical convective heat transfer coefficient can be estimated through the Nusselt number as described by Eq. 6 [19]:

$$Nu = CRe^{0.66}Pr^{0.33}\left(\frac{\mu_w}{\mu}\right)^{-0.14} \quad (6)$$

Where C is a constant which can range from 0.4 to 0.8 for anchor stirrers, Re is the Reynolds number for a stirred vessel, Pr is the Prandtl number of water at 64 °C (Pr = 2.8), μ_w is the viscosity of the film at the wall, and μ is the viscosity of the bulk fluid. For this estimate, all thermophysical properties were assumed constant with water at 64 °C based on [16]. Additionally, it was assumed that there was a negligible difference in the wall and bulk viscosities ($\mu_w = \mu$). Application of Eq. (6) estimated $Nu \approx 710 - 1420$ and $h_{conv} \approx 2600 - 5200$ W/m²K for the range of C from 0.4 – 0.8, respectively, for a tank diameter of 0.18 m. Therefore, the estimated values of h_{conv} from the experimental work (Figure 13A) are much lower than the theoretical estimates of h_{conv}. There are several possible explanations for the discrepancy between the experimental and theoretical h_{conv}: (1) the liquid level height to vessel diameter ratio ($H/D = 0.78$) does not conform to most favorable, theoretical aspect ratio ($H/D = 1$) which is assumed by the theoretical estimate of h_{conv}, (2) the assumption of constant heat flow ($\dot{Q}$, Figure 5) between the two calibration states may be invalid due to an increase in axial heat flow with the addition of an artificial fouling layer (i.e., 0.5 mm of PTFE) to the surface of the finger, and (3) there may be uncertainty in the estimated thermal conductivities in Table 1 used to estimate R_0 and R_1 (Eq. 4).

Finally, the calibration method was applied to calculate the step-wise change in thermal resistance at different retraction heights with the addition of artificial fouling layers below the liquid surface (Figure 14). The addition of 0.5 mm of PTFE is indicated by points B, D, and F in Figure 14A, corresponding to total PTFE thicknesses of 0.5, 1, and 1.5 mm, respectively. This process is also visualized in Figure 4. The thermal resistance of the fouling layer was computed using the estimated real heat flow through the sample plate and the experimentally estimated h_{conv} (Figure 13) and plotted in Figure 14B.

ISBN: 978-0-9984188-3-4; Published online www.heatexchanger-fouling.com

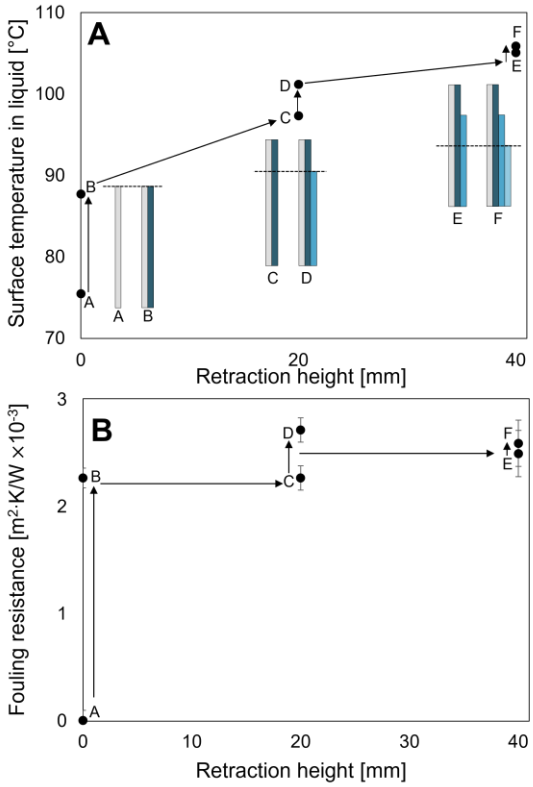

Figure 14. (A) Change in surface temperature and (B) fouling resistance for step-wise thermal resistance addition of multiple layers of 0.5 mm of PTFE. The points of PTFE addition are illustrated by the sketches in (A and Figure 4). Error bars in (B) are associated with uncertainty in the h_{conv}, not replication.

Figure 14A shows an overall increase in temperature with the retraction and addition of PTFE fouling layers, but there is a decrease in the temperature change with the subsequent addition of PTFE fouling layers (e.g., $T_B - T_A$ vs. $T_D - T_C$). This is an unexpected result because the temperature change associated with the addition of subsequent layers of PTFE (i.e., at 20 and 40 mm) should be greater than the temperature change at 0 mm (12.3 K) due to the expected increased flux in the liquid phase.

The decreasing temperature change at increasing retraction heights is also reflected in the predicted thermal resistance of the fouling layer (Figure 14B). The first step (A to B) describes the estimated thermal resistance of the 0.5 mm thick PTFE (~2.0 m^2·K/W, Table 1), but this is expected as these two states (A and B) were used for calibration. For a retraction height of 20 mm (C to D), the fouling resistance is severely underpredicted and there is almost no change in the predicted fouling resistance at a retraction height of 40 mm (E to F).

To attempt to explain these discrepancies, a deeper analysis of the distribution of surface temperatures in liquid for the conditions described in Figure 14 is depicted in Figure 15.

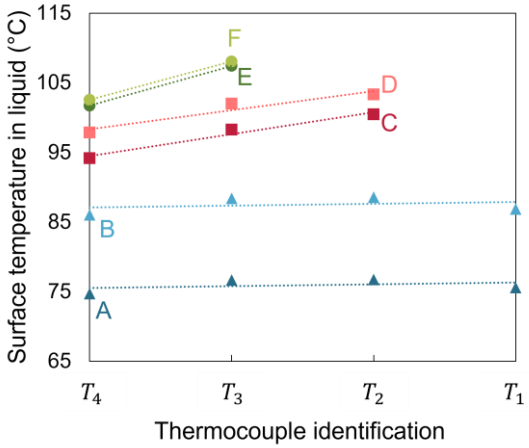

Figure 15.Change in the surface temperature in liquid for step-wise thermal resistance method depicted in Figure 14A. The letters A-F match the respective retraction and thermal resistance situations described in Figure 14A. Only the thermocouples from the low flow face are plotted and the locations of $T_1 - T_4$ are described in Figure 2B.

Figure 15 illustrates that with increasing retraction, the gradient between adjacent thermocouples submerged in liquid increases. Heat flow exists when a temperature gradient is present with heat flowing from a region of high temperature to a region of lower temperature. This suggests a need to reconsider the estimation of the axial heat flow which was estimated in *Commissioning Test #1* (Figure 10B). As previously discussed, this estimation is only expected to reflect the trend in axial heat flow with retraction, but not the actual magnitude.

Additionally, given the difference between the theoretical and experimental values of h_{conv}, there may be a need to revise the calibration protocol in future work. The protocol presented in this work relies on a 2-point calibration with the use of two thermal resistance states (R_0 and R_1). But additional data points could be added between R_0 and R_1 such that a multi-point calibration could be conducted. A linearization of the steady state heat transfer equation with R_f as the dependent variable and T_s as the response variable is described in Eq. (7):

$$T_s = \left(\dot{q} \cdot \frac{1}{h_{conv}} + T_b\right) + \dot{q} \cdot R_f \qquad (7)$$

A linear regression with Eq. (7) enables determination of the heat flux ($\dot{q}$) from the slope and h_{conv} from the y-intercept ($\dot{q} \cdot \frac{1}{h_{conv}} + T_b$). This modification to the calibration protocol could also be used to test the assumption of equal heat flows between the clean and artificially fouled states (i.e., the contribution of axial heat flow). A curve of T_s vs. R_f should show a linear trend if there is limited axial heat flow.

ISBN: 978-0-9984188-3-4; Published online www.heatexchanger-fouling.com

CONCLUSIONS & OUTLOOK

This work focuses on the design and experimental setup of a movable heated finger for the study of fouling during an emulsion polymerization reaction. An electric prototype finger proved to be advantageous, compared to a fluidic prototype finger, due to its versatility in multiple modes of operation and sensitivity in power and surface temperature measurements.

The prototype electric finger was upgraded with a new design which proved to have better heat distribution. The redesigned finger also had an increased number of temperature measurement points compared to the prototype finger to support 'movable' functionality. The first tests of the redesigned heated finger in water indicated that a constant surface temperature below the surface of the liquid could be maintained, even during retraction of the finger into air. Furthermore, the power needed to maintain a constant surface temperature was directly proportional to the surface area exposed to air. The application of the redesigned heated finger for the quantitation of fouling of a preformed latex indicated a higher fouling rate under a constant heat flux operation compared to a constant surface temperature operation. This was explained by the constant temperature of the surface of the deposit exposed to bulk fluid flow for the constant heat flux operation.

A calibration method with artificial PTFE fouling layers was presented to estimate the convective heat transfer coefficient in liquid. The experimental convective heat transfer coefficient was found to be dependent on the retraction height. But significant deviations between the experimental and theoretical estimates of the convective heat transfer coefficient emphasize the need to reevaluate the impact of axial heat flow and the assumptions of the calibration protocol in future investigations. A multi-point calibration method, rather than the two-point calibration method used in this study, was proposed and will be the subject of future work. Additionally, future investigations will consider the application of insulation to the base of the finger and the installation of a heat flux sensor for axial heat flow measurements.

ACKNOWLEDGEMENTS

This work is funded by Deutsche Forschungsgemeinschaft (DFG, Project Number: 504119618). All polymerization chemicals were kindly provided by Wacker Chemie AG. The authors would like to thank Jörg Leppelt, Karl Karrenführer, and Sven Lorenzen for their electrical and mechanical assistance with this work.

NOMENCLATURE

A_c	Cross sectional flow area, m^2
A_s	Surface area, m^2
c_p	Specific heat, J/kg·K
D	Diameter, mm
D_i	Inner diameter, mm
D_o	Outer diameter, mm
h_{conv}	Convective heat transfer coefficient, W/m^2·K
k	Thermal conductivity, W/m·K
$\dot{m}$	Mass flow rate, kg/s
n	Number of replicates, [-]
Pr	Prandtl number, [-]
$\dot{Q}$	Heat flow, W
$\dot{q}$	Heat flux, kW/m^2
R	Heat transfer resistance, m^2·K/W
Re	Reynolds number, [-]
t	time, s or min
T	Temperature, °C
U	Overall heat transfer coefficient, W/m^2·K
z	Distance, m
μ	Viscosity, Pa·s
ρ	Density, kg/m^3
θ	Dimensionless temperature difference, [-]

Subscripts

b	bulk fluid
c	cross sectional
conv	convection
f	fouling
i	inlet fluid
o	outlet fluid
s	surface
w	wall
0	initial (time = 0) or clean
1…8	thermocouple identifier

REFERENCES

[1] Odian, G., *Principles of polymerization*, 4th ed., Wiley. Hoboken, NJ, USA. 2010. (book)

[2] Hohlen, A., Augustin, W., & Scholl, S. Quantification of Polymer Fouling on Heat Transfer Surfaces During Synthesis, *Macromolecular Reaction Engineering*, 14(1), Article 1900035, 2020. (article)

[3] Hohlen, A., Ablagerungsmechanismen einer Polymerdispersion auf wärmeübertragenden Oberflächen während der Emulsionspolymerisation. PhD thesis, Technische Universität Braunschweig, Germany, 2022. (thesis)

[4] Urrutia, J., Peña, A., & Asua, J. M., Reactor Fouling by Preformed Latexes., *Macromolecular Reaction Engineering*, 11(1), Article 1600043. 2017. (article)

[5] Urrutia, J., & Asua, J. M., Reactor Fouling in Emulsion Polymerization, *Industrial & Engineering Chemistry Research*, 60(29), 10502–10510, 2021. (article)

[6] Klinkert, A., Friedrich, Z., Glatt, E., Augustin, W., & Scholl, S., Polymer Versus Polymerization Fouling: Basic Deposition Mechanisms During Emulsion Polymerization by the Example of a Vinyl Acetate and Versa 10 Copolymer, *Macromolecular Reaction Engineering*, Article 2300057, 2024. (article)

[7] Böttcher, A., Petri, J., Langhoff, A., Scholl, S , Augustin, W, Hohlen, A., & Johannsmann, D., Fouling Pathways in Emulsion Polymerization

ISBN: 978-0-9984188-3-4; Published online www.heatexchanger-fouling.com

Differentiated with a Quartz Crystal Microbalance (QCM) Integrated into the Reactor Wall, *Macromolecular Reaction Engineering*, Article 2100045, 2022. (article)

[8] Besevic, P., Clarke, S. M., Kawaley, G., & Wilson, D. I., A Novel fouling Cell to Study Influence of Solution on Crystallisation Fouling, *Heat Exchanger Fouling and Cleaning Conference*, Madrid, Spain, 2017. (proceedings)

[9] Karela, A., Clarke, S. M., Kawaley, G., Routh, A. F., & Wilson, D. I., Freezing fouling from aqueous solutions of TBAB and TME clathrate hydrates, *Chemical Engineering Science*, 263, 117923. 2022. (article)

[10] Kasumu, A. S., & Mehrotra, A. K., Solids Deposition from Wax–Solvent–Water "Waxy" Mixtures Using a Cold Finger Apparatus, *Energy & Fuels*, 29(2), 2015. (article)

[11] Jennings, D. W., & Weispfennig, K., Effects of Shear and Temperature on Wax Deposition: Coldfinger Investigation with a Gulf of Mexico Crude Oil, *Energy & Fuels*, 19(4), 1376–1386. 2005. (article)

[12] Geddert, T., Augustin, W., & Scholl, S., Induction Time in Crystallization Fouling on Heat Transfer Surfaces. *Chemical Engineering & Technology*, 34(8), 1303–1310, 2011. (article)

[13] Kuschnerow, J. C., Dorn, S., Föste, H., Augustin, W., & Scholl, S., Investigations of Polymer Fouling on Heated and Cooled Surfaces, *Heat Exchanger Fouling and Cleaning Conference*, Budapest, Hungary, 2013. (proceedings)

[14] Schnöing, L., Shahnazari, R. N., Hohlen, I., van Asselt, A. J., Augustin, W, & Scholl, S., Alkaline cleaning of ultra-high temperature dairy fouling in a laminar flow regime, *International Dairy Journal*, 117, 105014, 2021. (article)

[15] Schnöing, L., Wiese, H., Tran, T.T., van Asselt, A. J., Augustin, W, & Scholl, S. Interaction of alkaline and acid treatment on the removal of proteinaceous mineral-enriched dairy fouling from UHT treatment, *International Dairy Journal*, 152, 105876, 2024. (article)

[16] Linstrom, Peter (1997): NIST Chemistry WebBook, NIST Standard Reference Database 69. National Institute of Standards and Technology. (webbook)

[17] Verein Deutscher Ingenieure VDI-Gesellschaft Verfahrenstechnik und Chemieingenieurwesen (GVC), VDI Heat Atlas (Second Edition) Springer Berlin Heidelberg, 2010. (book)

[18] Tsai, J.H., Cuckston, G., Schnöing, L., Augustin, W., Scholl, S., Hallmark, B., Wilson, I. (2022): Fluid Dynamic Gauging for Studying Early Stages of Swelling of Fouling Deposits, *Heat Transfer Engineering*, 43 (15-16), pp. 1378–1386. 2022. (article)

[19] Zlokarnik, Marko. *Stirring. Theory and Practice*. Wiley-VCH, Weinheim, NY, USA, 2001. (book)

ISBN: 978-0-9984188-3-4; Published online www.heatexchanger-fouling.com